

# Parallel Accelerated Custom Correlation Coefficient Calculations for Genomics Applications<sup>☆</sup>

Wayne Joubert<sup>a,\*</sup>, James Nance<sup>a</sup>, Sharlee Climer<sup>c</sup>, Deborah Weighill<sup>a,b</sup>, Daniel Jacobson<sup>a,b</sup>

<sup>a</sup> Oak Ridge National Laboratory, 1 Bethel Valley Road, Oak Ridge, TN 37831

<sup>b</sup> The Bredesen Center for Interdisciplinary Research and Graduate Education, University of Tennessee, Knoxville, 444 Greve Hall, 821 Volunteer Blvd. Knoxville, TN 37996-3394

<sup>c</sup> University of Missouri-St. Louis, 1 University Blvd. 311 Express Scripts Hall, St. Louis, MO 63121-4400

---

## Abstract

The massive quantities of genomic data being made available through gene sequencing techniques are enabling breakthroughs in genomic science in many areas such as medical advances in the diagnosis and treatment of diseases. Analyzing this data, however, is a computational challenge insofar as the computational costs of the relevant algorithms can grow with quadratic, cubic or higher complexity—leading to the need for leadership scale computing. In this paper we describe a new approach to calculations of the Custom Correlation Coefficient (CCC) between Single Nucleotide Polymorphisms (SNPs) across a population, suitable for parallel systems equipped with graphics processing units (GPUs) or Intel Xeon Phi processors. We describe the mapping of the algorithms to accelerated processors, techniques used for eliminating redundant calculations due to symmetries, and strategies for efficient mapping of the calculations to many-node parallel systems. Results are presented demonstrating high per-node performance and near-ideal parallel scalability with rates of more than nine quadrillion ( $9 \times 10^{15}$ ) elementwise comparisons achieved per second with the latest optimized code on the ORNL Titan system, this being orders of magnitude faster than rates achieved using other codes and platforms as reported in the literature. Also it is estimated that as many as 90 quadrillion ( $90 \times 10^{15}$ ) comparisons per second may be achievable on the upcoming ORNL Summit system, an additional 10X performance increase. In a companion paper we describe corresponding techniques applied to calculations of the Proportional Similarity metric for comparative genomics applications.

**Keywords:** High performance computing, parallel algorithms, NVIDIA<sup>®</sup> GPU, Intel<sup>®</sup> Xeon Phi, comparative genomics, vector similarity metrics, Custom Correlation Coefficient,  
**2010 MSC:** 65Y05 [Computer aspects of numerical algorithms: Parallel computation], 68W10 [Algorithms: Parallel algorithms]

---

## 1. Introduction

Computation of the mathematical relationships between pairs of vectors is required in many science domains. In the field of genomics, the Custom Correlation Coefficient (CCC) [1] was developed to calculate

---

<sup>☆</sup>This manuscript has been authored by UT-Battelle, LLC under Contract No. DE-AC05-00OR22725 with the U.S. Department of Energy. The United States Government retains and the publisher, by accepting the article for publication, acknowledges that the United States Government retains a non-exclusive, paid-up, irrevocable, world-wide license to publish or reproduce the published form of this manuscript, or allow others to do so, for United States Government purposes. The Department of Energy will provide public access to these results of federally sponsored research in accordance with the DOE Public Access Plan (<http://energy.gov/downloads/doe-public-access-plan>).

Accepted to *Parallel Computing*, 5/16/18. © 2018. This manuscript version is made available under the CC-BY-NC-ND 4.0 license <http://creativecommons.org/licenses/by-nc-nd/4.0/>.

\*Corresponding author

Email address: [joubert@ornl.gov](mailto:joubert@ornl.gov) (Wayne Joubert)

the correlation between mutations, or Single Nucleotide Polymorphisms (SNPs), across a population of individuals. This can be used to identify groups of SNP alleles which tend to co-occur in a population and consequently can be used to find combinations of SNP alleles which associate with certain phenotypes, such as a disease phenotype [2]. CCC also takes into account genetic heterogeneity and finds correlations between SNP alleles which co-occur in portions of the population, not requiring co-occurrence across the whole population.

The effectiveness of CCC has been demonstrated in diverse domains. It has been used to identify genetic patterns exhibiting highly significant associations with both hypertensive heart disease [1] and psoriasis [2]. In another study, CCC was utilized to reveal genetic coadaptation between vitamin D receptor and skin color genes, suggesting parallel selective responses to environmental transitions as humans ventured out of Africa [3]. Interestingly, the CCC analysis of HapMap [4] data revealed a large-scale genetic pattern on human chromosome 14 [5]. This discovery suggests that two completely divergent evolutionary paths rapidly progressed in our past, presumably achieving the shared goal of enhancing gephyrin, a gene that is vital for signal transmissions in the human brain. Note that the HapMap data are arguably the most extensively studied SNP data available, yet this pattern was not previously identified by others—demonstrating CCC’s ability to identify combinatorial patterns of correlated SNP alleles within genome-wide data that are missed by other methods.

The explosive growth in genomic data has opened unprecedented levels of opportunity for addressing fundamental questions of importance in genomic sciences. However, the requisite computational methods are expensive, insofar as the computational complexity of general pairwise vector comparison methods is quadratic in the number of vectors, and the complexity is even higher for methods comparing three or more vectors at a time as is required in some cases. To perform large scale studies, it has thus become necessary to use high performance leadership computing systems possessing thousands of compute nodes equipped with advanced hardware such as accelerated manycore processors.

In this paper we describe new approaches to performing CCC calculations on leadership class systems equipped with GPUs. We describe implementations of CCC methods which attain high absolute performance on GPUs, use asynchronous methods to overlap operations, avoid the performance penalty of performing redundant and unnecessary computations, and exhibit near-ideal scaling to thousands of compute nodes.

Substantial recent work has focused on the problem of comparing pairs, triples or larger subsets of a set of vectors efficiently by means of advanced computational methods such as the use of parallelism, accelerated GPU or Intel Xeon Phi processing, or both. A broad overview of epistasis detection in comparative genomics including computational issues pertaining to parallelism and GPU acceleration is given in [6]. The GBOOST code, discussed in [7], is a gene-gene interaction code for 2-way studies optimized for single GPUs using encoding of gene data into bit strings with avoidance of redundant computations; Wang et al. [8] describes GWISFI, a single-GPU code for 2-way GWAS calculations. Gonzalez-Dominguez et al. [9] develops a UPC++ code for gene-gene interaction studies for small numbers of GPUs and Intel Phi processors exploiting vector hardware and hardware population count instructions. Gonzalez-Dominguez and Schmidt [10] considers 3-way interactions on a node with 4 GPUs. Solomonik et al. [11] develops parallel tensor computation methods, structurally similar to 3-way metrics computations, with particular attention to avoiding redundant computations; however, the work does not consider GPUs or shaping of the computational regions to accommodate processors with long vector lengths. Haque et al. [12] discusses similarity metric calculations for chemical informatics applications on single GPUs using space filling curve methods and hardware population count instructions; it recognizes the correspondence of these calculations to BLAS-3 matrix-matrix product computations and pays close attention to optimizing memory accesses. Wang et al. [13] considers 2-way studies on compute clouds using MapReduce on conventional CPUs. Yang et al. [14] adapts existing packages to perform 2-way CPU and GPU studies and 3-way CPU studies on as many as 200 cores in parallel. Goudey et al. [15] performs  $k$ -way GWAS studies for arbitrary  $k$  with consideration of load balancing and elimination of redundancies on a 4096-node IBM Blue Gene/Q system; results for a single GPU are also presented. Luecke et al. [16] performs 2-way analyses on up to 126 nodes of the Intel Phi-based Stampede system (cf. [17]). Koesterke et al. [18] considers 2-way computations on thousands of compute cores with good scalability and good absolute performance on conventional CPUs. Finally, recent work in [19] considers  $k$ -selection similarity search methods with applications to image data

with results for small numbers of GPUs; that work however focuses primarily on the  $k$ -selection problem for nonexhaustive inexact similarity search, a different problem from what is considered here.

This work is to our knowledge the first successful effort to combine all the needed elements for performing large-scale 2-way and 3-way vector comparison studies on leadership-class systems, including: high performance usage of accelerated processors, effective use of deep memory hierarchies, avoidance of unneeded redundant computations, effective scaling to thousands of compute nodes, and algorithm structuring to enable efficient I/O.

The remainder of this paper is organized as follows. After describing the 2-way and 3-way CCC methods in Section 2, we describe the techniques used to map these methods to GPUs and other manycore accelerated processors in Section 3. Then we describe the parallelization techniques applied to these methods in Section 4, followed by implementation details in Section 5. Computational results on the 27 petaflop Oak Ridge National Laboratory (ORNL) Cray XK7 Titan system are presented in Section 6. Discussion of future work is presented in Section 7, and conclusions are given in Section 8.

For additional discussion of shared topics pertaining to the algorithms and their implementations, it is advised that this paper be read in tandem with the companion paper [20].

## 2. The Custom Correlation Coefficient

### 2.1. The 2-way metric

We assume a set of  $n_v$  vectors of length  $n_f$  elements  $\{v_i\}_{i=1}^{n_v}$  with  $v_i \in (S_2)^{n_f}$  and  $v_i = \{v_{i,q}\}_{q=1}^{n_f}$ . Here  $S_2 = S \times S = S^2$  where  $S = \{0, 1\}$ , thus each vector entry  $v_{i,q}$  is itself a vector with two entries  $\{(v_{i,q})_r\}_{r=1}^2$  taken from  $S$ . In practice, the  $v_i$  are SNPs each of whose entries  $v_{i,q} \in S_2$  represents a pair of alleles, with a possibly different allele interpretation for each column  $i$ , and  $n_f$  is the number of samples or population size.

For  $a, b \in S$  define the indicator function  $\chi_a$  by  $\chi_a(b) = 1$  if  $a = b$ , otherwise 0. Let  $\rho_{i,q}(a) = \sum_r \chi_a((v_{i,q})_r)$ , the count of entries with the value  $a$  in  $v_{i,q}$ . The frequency of allele  $a$  for SNP  $v_i$  is then

$$f_i(a) = \frac{1}{2n_f} \sum_{q=1}^{n_f} \rho_{i,q}(a). \quad (1)$$

Clearly  $f_i(0) + f_i(1) = 1$ . Also let  $\rho_{i,j,q}(a, b) = \rho_{i,q}(a) \cdot \rho_{j,q}(b)$  and

$$f_{i,j}(a, b) = \frac{1}{4n_f} \sum_{q=1}^{n_f} \rho_{i,j,q}(a, b). \quad (2)$$

Note  $\sum_{a,b \in S} f_{i,j}(a, b) = 1$ . Then the 2-way CCC comparison for  $a, b \in S$  assuming a fixed constant  $\gamma = 2/3$  is

$$CCC_{i,j}(a, b) = f_{i,j}(a, b)(1 - \gamma f_i(a))(1 - \gamma f_j(b)). \quad (3)$$

The functions  $f_{i,j}()$ , and thus  $CCC_{i,j}()$ , are symmetric in  $i$  and  $j$ . Thus to compute all unique values  $\{f_{i,j}(a, b)\}_{i,j,a,b}$  for distinct  $i$  and  $j$  requires  $4n_f n_v (n_v - 1)/2 = O(n_f n_v^2)$  operations. On the other hand,  $\{f_i(a)\}_{i,a}$  requires only  $2n_f n_v = O(n_f n_v)$  operations. Due to its greater computational cost, the efficient calculation of  $\{f_{i,j}(a, b)\}$  will be the chief focus of this work.

An interpretation of the  $f_{i,j}$  component of the 2-way CCC calculation is shown in Figure 1. Here we let  $n_f = 1$  and  $n_v = 2$ . For the first entry of  $v_1$  and of  $v_2$ , each containing two binary entries as shown, all four pairings of the left two entries and the right two entries are selected and enumerated, with four resulting tuple values, each taken from a set of four possible combinations (0, 0), (0, 1), (1, 0) and (1, 1). These tuples are then tallied by value to count the frequency of each possible tuple. For the general case of  $n_f > 1$ , the additional entries are handled in the same way, with the counts of each pairing tally summed into the result table shown at the right.

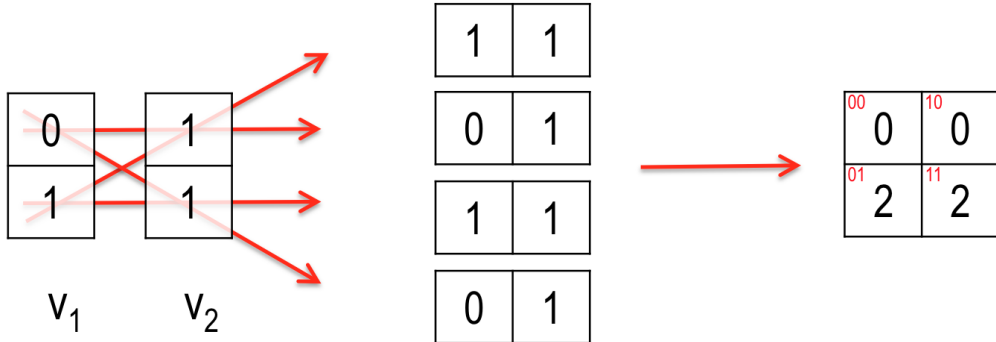


Figure 1: 2-way CCC calculation example. Left: two vectors of length 1, with each entry a 2-vector. Center: enumeration of all pairings of entries. Right: tallying of counts of each pairing type.

## 2.2. The 3-way metric

The previous section described CCC for evaluating pairs of SNPs; next we expand this to the evaluation of SNP trios. The 3-way CCC comparison for  $a, b, c \in S$  and vectors  $v_i, v_j, v_k$  and a fixed constant  $\gamma$  is defined by

$$CCC_{i,j,k}(a, b, c) = f_{i,j,k}(a, b, c)(1 - \gamma f_i(a))(1 - \gamma f_j(b))(1 - \gamma f_k(c)). \quad (4)$$

Here,

$$f_{i,j,k}(a, b, c) = \frac{1}{8n_f} \sum_{q=1}^{n_f} \rho_{i,j,k,q}(a, b, c) \quad (5)$$

for  $\rho_{i,j,k,q}(a, b, c) = \rho_{i,q}(a) \cdot \rho_{j,q}(b) \cdot \rho_{k,q}(c)$ .

Due to symmetries in  $i, j$  and  $k$ , only  $8n_v(n_v - 1)(n_v - 2)/6$  unique values of  $\{f_{i,j,k}(a, b, c)\}_{i,j,k,a,b,c}$  need be computed for distinct  $i, j$  and  $k$ , requiring  $8n_f n_v(n_v - 1)(n_v - 2)/6 = O(n_f n_v^3)$  operations. The dominance of this computational expense over the calculation of the  $f_i(a)$  values makes this the primary focus of attention.

Figure 2 gives an interpretation, for  $n_f = 1$  and  $n_v = 3$ . Again, each vector has one entry which is itself a 2-vector of binary entries. All eight combinations of vector entries are sampled, and the counts of these triples are tallied into a table whose entries correspond to the eight possible combinations of three binary values.

## 3. Mapping to manycore processors

### 3.1. The 2-way metric

Let us define  $B = V^T \circ_2 V$  to satisfy  $(B_{i,j})_{a,b} = f_{i,j}(a, b)$ , so that each entry of  $B$  is a  $2 \times 2$  tally table. It can be observed that the basic structure of the computation of the  $f_{i,j}(a, b)$  values—namely, the summing of values derived from corresponding entries of each pair of vectors—is identical to the structure of the general matrix-matrix product computation (GEMM), with the pairwise multiplication of scalar vector elements in the GEMM replaced with a tally into a  $2 \times 2$  table. To solve this efficiently on manycore compute nodes, we follow the approach of [20], adapting the GEMM kernel from an optimized dense linear algebra library, in this case MAGMA[21] targeting GPUs, to accelerate this operation.

In [20] we implemented the Proportional Similarity metric by replacing the scalar multiplication operation of the GEMM with the operation of taking the minimum of two scalar values. Here however we have a tally operation which requires special considerations to implement efficiently. For CCC, since every entry of

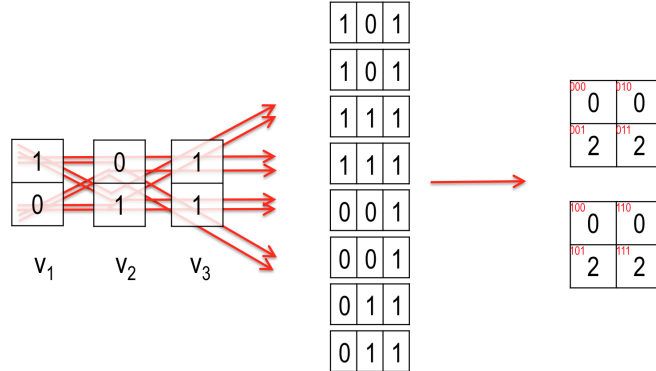


Figure 2: 3-way CCC calculation example. Left: three vectors of length 1, with each entry a 2-vector. Center: enumeration of all combinations of entries. Right: tallying of counts of each combination type.

$v_i$  is composed of only two bits, significant savings in computation time as well as storage is possible by packing the bits of many vector entries into a single compute word. We use the MAGMA double complex ZGEMM operation, for which each MAGMA vector entry is composed of two 64-bit words, so that a single ZGEMM vector entry can hold 64  $v_i$  entries. For fixed  $i$  and  $j$ , four  $f_{i,j}(a,b)$  (integer) values must then be accumulated. To fit this into a result value of two 64-bit doubles for the ZGEMM, we assign 25 bits of the mantissa of each of the two floating point numbers to store each result. This allows  $n_f$  to be as large as  $2^{23} - 1 = 8,388,607$ , without loss of precision from overflow of the mantissa or mixing of the two integer components stored in each word. This limit is far above the typical requirements for the targeted calculations. The resulting modified ZGEMM operation we refer to here as mGEMM2.

For each pair of corresponding double complex vector entries for which a tally is performed, it is efficient to use bitwise operations. In the implementation, to accumulate to tally targets (0, 0), (0, 1), (1, 0) and (1, 1), corresponding words are operated on by left and right bit shifts and bitwise OR and AND operations to obtain words for which each bit is set to 1 if the original pair of bits corresponds to the respective tally table entry and 0 otherwise. Then the CUDA intrinsic `__popc11()` corresponding to a hardware population count operation is used to sum the number of bits of the word set to 1 and accumulate the result. The population count operation is supported in hardware for some conventional x86 CPUs as well; if not, it can typically be implemented with small numbers of machine instructions; see for example [22], [23]. In the implementation, care must be taken for the case when  $n_f$  is not a multiple of 64 so that the tallies corresponding to the zero padding are corrected for.

Though we do not pursue the topic here, it is likely that libraries optimized to other processor architectures, such as PLASMA [24], BLIS [25] and OpenBLAS [26] would provide similar opportunities for high performance for conventional processors and Intel Xeon Phi.

### 3.2. The 3-way metric

The 3-way method cannot be mapped directly to a modified GEMM framework using the same approach, insofar as in this case the tally table entries would need to be reduced to 12 bits to fit into two double precision words of the ZGEMM, limiting  $n_f$  to size 4095 or less, inadequate for many problems. Thus an alternative approach is needed.

To solve this problem, the basic approach taken here is a two-step process. First, for given  $V$  and a fixed column  $v_j$  we construct modified matrices  $X_{j,\xi}$ ,  $1 \leq \xi \leq 3$ , each of the same dimension as  $V$ . Second, we calculate  $B_\xi = X_{j,\xi}^T \circ_3 V$  for an operator  $\circ_3$  representing a modified 2-way calculation from which it is possible to reconstruct the 3-way tally values for  $v_i$ ,  $v_j$  and  $v_k$ , for  $1 \leq i, k \leq n_v$ .

For the first step, the entry  $(X_{j,\xi})_{q,p}$  is formed from the entries  $v_{j,q}$  and  $(V)_{q,p}$  according to the rules shown in Table 1. The table gives values for the  $n_f = 1$  case; for the general case, corresponding rows of  $v_j$  and  $V$  are handled likewise. Here, for convenience the entries of  $v_j$  and  $V$  that have the value (1, 0) are

Table 1: Values of  $X_{j,\xi}$ 

$V$	$v_j$	$X_{j,1}$	$X_{j,2}$	$X_{j,3}$
0,0	0,0	0,0	1,0	1,0
0,0	0,1	0,1	1,0	1,0
0,0	1,1	1,1	1,0	1,0
0,1	0,0	1,0	0,0	1,0
0,1	0,1	1,0	0,1	1,0
0,1	1,1	1,0	1,1	1,0
1,1	0,0	1,0	1,0	0,0
1,1	0,1	1,0	1,0	0,1
1,1	1,1	1,0	1,0	1,1

omitted since they have an identical result on the calculation as  $(0, 1)$  insofar as the CCC result tally values do not differentiate between these cases.

The aim here is, for each column of  $V$  (with  $(1, 0)$  entries mapped to  $(0, 1)$ ), to form the corresponding columns of  $X_{j,1}$ ,  $X_{j,2}$  and  $X_{j,3}$  by taking the corresponding entry of  $v_j$  (again replacing  $(1, 0)$  with  $(0, 1)$ ) if the corresponding entry of the  $V$  column equals  $(0, 0)$ ,  $(0, 1)$  and  $(1, 1)$  respectively, and the “null” indicator value of  $(1, 0)$  otherwise. We refer to this modified GEMM operation as mGEMM3.

After  $\{X_{j,\xi}\}_\xi$  are formed, the matrices  $B_{j,\xi} = X_{j,\xi}^T \circ_3 V$  are calculated similarly to the previously described 2-way method based on modified GEMMs. Here the operator  $\circ_3$  represents the same tally process as used for the 2-way method described above except that  $X_{j,\xi}$  values equal to the null indicator  $(1, 0)$  are discarded and not used in the tally.

It is then straightforward to construct the 3-way tallies from the constituent 2-way tallies  $\{B_{j,\xi}\}_\xi$ . The matrix  $B_{j,1}$  contributes tallies for entries of  $V$  equal to  $(0, 0)$ , and similarly  $B_{j,2}$  for  $(0, 1)$  and  $B_{j,3}$  for  $(1, 1)$ . For each  $B_{j,\xi}$ ,  $1 \leq \xi \leq 3$ , the four 2-way tally results for each vector triple must be mapped to the appropriate eight table entries for the 3-way tally associated with this vector triple. The mapping of contributions for each  $\xi$  is given by

$$\begin{aligned}
f_{i,j,k}(0, 0, 0) &= 2((B_{j,1})_{(i,k)})_{(0,0)} + ((B_{j,2})_{(i,k)})_{(0,0)}, \\
f_{i,j,k}(0, 0, 1) &= 2((B_{j,1})_{(i,k)})_{(0,1)} + ((B_{j,2})_{(i,k)})_{(0,1)}, \\
f_{i,j,k}(0, 1, 0) &= 2((B_{j,1})_{(i,k)})_{(1,0)} + ((B_{j,2})_{(i,k)})_{(1,0)}, \\
f_{i,j,k}(0, 1, 1) &= 2((B_{j,1})_{(i,k)})_{(1,1)} + ((B_{j,2})_{(i,k)})_{(1,1)}, \\
f_{i,j,k}(1, 0, 0) &= 2((B_{j,3})_{(i,k)})_{(0,0)} + ((B_{j,2})_{(i,k)})_{(0,0)}, \\
f_{i,j,k}(1, 0, 1) &= 2((B_{j,3})_{(i,k)})_{(0,1)} + ((B_{j,2})_{(i,k)})_{(0,1)}, \\
f_{i,j,k}(1, 1, 0) &= 2((B_{j,3})_{(i,k)})_{(1,0)} + ((B_{j,2})_{(i,k)})_{(1,0)}, \\
f_{i,j,k}(1, 1, 1) &= 2((B_{j,3})_{(i,k)})_{(1,1)} + ((B_{j,2})_{(i,k)})_{(1,1)}.
\end{aligned}$$

The 3-way calculation thus requires three modified GEMM operations, compared to one for the 2-way method. Insofar as each 3-way vector triple tally requires eight values compared to four for each 2-way pair, and the path length (Figure 2) is three for the 3-way method compared to two for the 2-way method (Figure 1), we believe it is near-optimal for the 3-way method computed using bitwise arithmetic to require roughly 3X the work of the 2-way method, as is the case in this implementation.

## 4. Multi-node parallelism

The details of the parallel implementation are essentially identical to those for the Proportional Similarity metric as described in detail in [20]. Here we give the main ideas in summary form.

Parallelism is obtained by decomposing both the  $n_f$  problem dimension and the  $n_v$  problem dimension across  $n_{pf}$  and  $n_{pv}$  nodes respectively, resulting in  $n_{fp} \times n_{vp}$  elements per node. Here for convenience we assume one GPU per node, though the implementation does not require this. A third axis,  $n_{pr}$ , is used to apply additional parallelism across the computation of the result values.

The  $n_{pf}$  parallelism axis requires a parallel reduction operation. The  $n_{pv}$  axis requires carefully scheduled point-to-point communications so that every vector can be compared against every other vector.

For the 2-way method, the result values form a 2-D square matrix of values with an imposed decomposition into smaller square blocks due to the  $n_{pv}$  parallelism. To avoid computing redundant values resulting from symmetry of the matrix, results are computed only for a block circulant subset of the blocks. Each  $n_{pv}$ -parallelism compute node is responsible for computing a block row of this matrix. The  $n_{pr}$  parallel axis is used to parallelize the computation of the blocks of this block row.

For the 3-way method, the result values make up a cube-shaped 3-D array of values, implicitly decomposed into smaller cubes by the  $n_{pv}$  parallel decomposition. A scheme is implemented so that only a subset or “slice” of values is calculated for each block, this subset chosen to represent each of the unique values in the result exactly once. Each  $n_{pv}$ -parallelism compute node is responsible for computing a 2-D slab of the results cube. The  $n_{pr}$  axis of parallelism is deployed so that the blocks in this slab can be computed in parallel.

The 3-way method allows an additional setting,  $n_{st}$ , which allows the metrics computation to be broken into multiple stages. To reduce the main memory storage costs for the metrics values, a run can be performed for which only a single stage of results is computed.

Asynchronous methods are used to overlap GPU computations, CPU computations, communications and transfers of data to and from the GPUs.

## 5. Implementation

The algorithms described here are implemented in the CoMet parallel genomics code. This code is written in C++, compiles with the GNU compiler suite and depends on MPI, CUDA and the modified versions of the MAGMA library. GNU Make and CMake are used for build management, and googletest is used for unit testing. The clang-format source code tool from the clang compiler package is used for source code formatting, and Git is used for repository management.

OpenMP CPU threading is used to accelerate the parts of the computation that are not ported to the GPU by mapping execution to multiple CPU cores on the node; when possible, the CPU work is also hidden under the asynchronously launched GPU kernels to improve performance.

For making comparisons, each method has a reference (CPU-only) version, a (possibly optimized) CPU version, and a GPU version. A set of synthetic reference test cases is implemented for testing, designed to give the exact same bit-for-bit result for all code versions and for all parallel decompositions. Two types of synthetic problem are implemented: a version for which each vector entry is set to a randomized value, and a second version with randomized placement of entries specifically chosen so that the correctness of every result value can be verified analytically. A checksum feature using extended precision integer arithmetic computes a bit-for-bit exact checksum of computed results to check for errors when using synthetic inputs.

The code can be compiled under single or double precision. The precision setting for the CCC case affects only the accuracy of the calculation of the  $f_i()$  values for the denominators; for the numerator computations, as described earlier the relevant computations are performed with double complex data types operated on primarily with bitwise operations.

To modify MAGMA as needed for the algorithms, it is necessary to modify the two files in the MAGMA package `magmablas/gemm_stencil.cuh` and `magmablas/gemm_stencil_defs.h`. In particular, the macro definition for “`fma`” defining the fused multiply accumulate must be changed to make use of the appropriate tally operation.

## 6. Computational results

### 6.1. Overview

Experiments are performed on the ORNL Titan Cray XK7 system. Titan is composed of 18,688 compute nodes each equipped with an AMD Interlagos 16 core CPU and an NVIDIA Kepler K20X GPU connected via a PCIe-2 bus. The K20X GPU has peak single/double precision flop rate of 3,935/1,311 GF and peak memory bandwidth of 250 GB/sec. Each node contains 32 GB main memory and 6 GB GPU memory.

The software versions used are Cray OS version 5.2.82, Cray Programming Environment 2.5.13, GCC 4.9.3, MAGMA 1.6.2 and CUDA toolkit 7.5.18-1.0502.10743.2.1. For large node counts, it is in some cases necessary to set the environment variable `APRUN_BALANCED_INJECTION` to values such as 63 or 33 to avoid throttling of the communication network resulting from the algorithms’ communication patterns and causing performance loss.

The primary use of the code is to solve very large problems not previously solvable; thus weak scaling behavior, for which the work per node is kept roughly constant as compute node count is increased, is the primary focus.

GPU-enabled runs are executed with one MPI rank and one GPU per Titan node. Reported execution times do not include I/O. The source code execution path for the algorithm is identical independent of the actual values contained in the input vectors; thus we expect performance for the synthetic datasets used here to be essentially identical to performance with actual genomics data.

### 6.2. Single GPU kernel performance

We first evaluate the raw performance of the modified GEMM kernels in comparison with the standard GEMM. We test the mGEMM2 and mGEMM3 operations described above, used for the 2-way and 3-way methods respectively. We use  $n_v = 10,240$  vectors of length  $n_f = 393,216$  2-bit values corresponding to 6,144 double complex values. Timings are compared against the standard ZGEMM for matrices of the same size in memory. Kernel times are taken from the CUDA Profiler and include kernel time only, without transfer or CPU times.

Results are shown in Table 2. Raw timings are shown as well as normalized times representing the time per pair of elements operated on, where an element is interpreted to be a double complex value except for the modified GEMM cases in which case it is a 2-bit value. The cost of mGEMM3 is higher than that of mGEMM2 due to additional integer masks and other operations needed. The modified GEMMs have 64X higher density of vector elements per double complex value, thus suggesting a higher throughput rate than ZGEMM is possible; however, instead of four fused multiply-add FMA operations per pair in the ZGEMM case, a significant number of bitwise operations such as shifts, masks, bitwise operations and population counts are required per element pair. Thus the modified GEMM normalized rates exceed the ZGEMM theoretical peak by a smaller value than expected. A side effect is that computational intensity is extremely high, suggesting potentially high processor utilization and favorable opportunities to hide communications and GPU data transfers under computations. The MAGMA ZGEMM rates are somewhat less than those of cuBLAS since the former is more targeted toward smaller cases required by other MAGMA operations. Possible further optimizations of the bitwise operations of the modified GEMMs will be a topic of further study.

### 6.3. Performance model

It is desirable to model algorithm performance in order to evaluate expected performance and also to give guidance regarding selection of tuning parameters. We assume here that mGEMM2 and mGEMM3 sizes are large enough to hide communications, GPU data transfers and CPU computations.

For the 2-way case, we define  $\ell$ , the “load,” to denote the number of blocks assigned to each node. Then the execution time of the algorithm is estimated by

$$t = t_C + t_{T,V} + \ell \cdot t_{G,2} + t_{T,M} + t_{CPU},$$



Table 2: Kernel performance for single GPU case

	time (sec)	time per element pair	element pairs per second
mGEMM2	163.901	1.716E-12	5.828e11
mGEMM3	217.294	2.453E-12	4.077e11
ZGEMM, MAGMA	6.998	10.863e-12	0.921e11
ZGEMM, cuBLAS	4.493	6.974e-12	1.434e11
ZGEMM, theoretical peak	3.931	6.102e-12	1.639e11

where  $t_C$  is the time for communicating  $n_{fp}n_{vp}$  vector elements per node for a parallel step,  $t_{T,V}$  the time to transfer  $n_{fp}n_{vp}$  vector elements to the GPU for a step,  $t_{T,M}$  the time to transfer  $n_{vp}^2$  metrics values from the GPU per step,  $t_{CPU}$  the time for denominator and quotient calculations per step and  $t_{G,2}$  the time for an mGEMM2 computation. The non-mGEMM2 times are included here to account for asynchronous pipeline startup and drain. It is evident that maximizing  $\ell$  (by limiting  $n_{pr}$ ) makes it possible to approach peak mGEMM2 performance. mGEMM2 rates are determined empirically; the goal is to make the matrix dimensions  $n_{fp}$  and  $n_{vp}$  for the mGEMM2 computation as large as possible to maximize mGEMM2 efficiency. This suggests for a given problem it is desirable to reduce  $n_{pv}$  and  $n_{pf}$  until CPU or GPU memory is filled.

For the 3-way case, we again define the load  $\ell$ , here representing the number of block slices computed by a node. Each slice is computed by a GPU pipeline of  $3(n_{vp}/6)/n_{st}$  mGEMM3 steps corresponding to the required three mGEMM3 operations to form each 3-way result. The execution time of the algorithm is estimated by

$$t = t_C + t_{T,V} + \ell \cdot [3((n_{vp}/6)/n_{st})t_{G,3} + t_{T,V} + t_{T,M} + t_{CPU}].$$

Here mGEMM3 performance is approached by increasing  $\ell$  and  $n_{vp}$ , and decreasing  $n_{st}$ , subject to memory constraints. Similarly to the 2-way case,  $n_{fp}$  and  $n_{vp}$  should be maximized in order to maximize mGEMM3 performance.

#### 6.4. 2-way results

For 2-way weak scaling results we set  $n_f = 358,000$  elements per vector and  $n_{vp} = n_v/n_{pv} = 4,096$  vectors per node. We set the load  $\ell = 25$  and set  $n_{pr} = \lceil [n_{pv}/2 + 1]/\ell \rceil$  and  $n_{pf} = 1$ . The 2-way test runs are executed on up to 17,955 of Titan’s 18,688 compute nodes, or 96.1% of the system.

Results are shown in Figure 3. The left graph shows good weak scaling timing performance up to the full system. The method benefits from the very high computational intensity of the mGEMM2 kernel, dominating communication costs which it asynchronously overlaps. The right graph shows good weak scaling performance for the comparison rate per node. The maximum rate per node is 507e9 comparisons per second per node. Here a comparison defined as the operation between corresponding vector elements that produces four tally values to be accumulated. This rate is 87% of the single node peak measured value of 582.8e9 from Table 2, indicating almost perfect efficiency at scale.

The method attains up to 9.11e15 comparisons (9.11 petacomparisons) of two vector elements per second. See Table 3.

#### 6.5. 3-way results

The 3-way test runs are executed on up to 18,424 of Titan’s 18,688 compute nodes, or 98.6% of the system. We use  $n_f = 20,000$  elements per vector and  $n_{vp} = n_v/n_{pv} = 2,880$  vectors per node. We set the load  $\ell = 6$ ,  $n_{pr} = \lceil (n_{pv} + 1)(n_{pv} + 2)/\ell \rceil$ , and  $n_{pf} = 1$  and compute the final stage of  $n_{st} = 16$  stages.

Weak scaling results are shown in Figure 4. The left graph shows near ideal weak scaling timing behavior for large problem sizes. The right graph shows the average number of vector element comparisons performed per second per node. Here one comparison is defined as a single 3-way calculation involving three vector elements that produces eight tallied results. Some inefficiencies exist a lower node counts due to known load

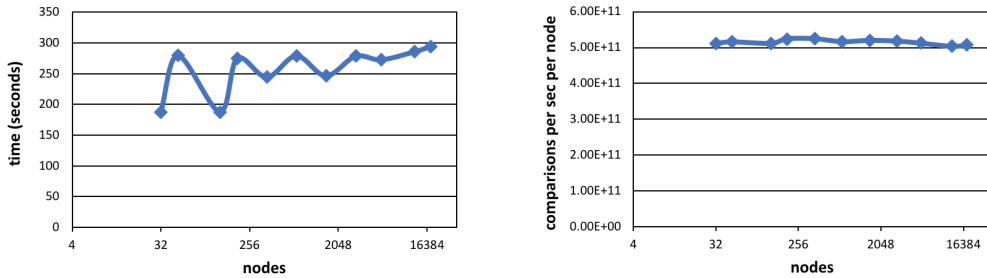


Figure 3: CCC 2-way weak scaling. Left: time to solution. Right: number of unique elementwise comparisons per second per node.

Table 3: Maximum performance, CCC

method	comparisons per second
2-way CCC	$9.11 \times 10^{15}$
3-way CCC	$2.06 \times 10^{15}$

balancing effects from the implementation; the effects are minimal at large node counts. The maximum rate per node is 112e9 comparisons per second; this is 82% of the peak single node measurable value of 136e9, this value being 1/3 of the 4.077e11 mGEMM3 value from Table 2 since three mGEMM3 operations are required for each result. Thus very high efficiency is achieved at scale.

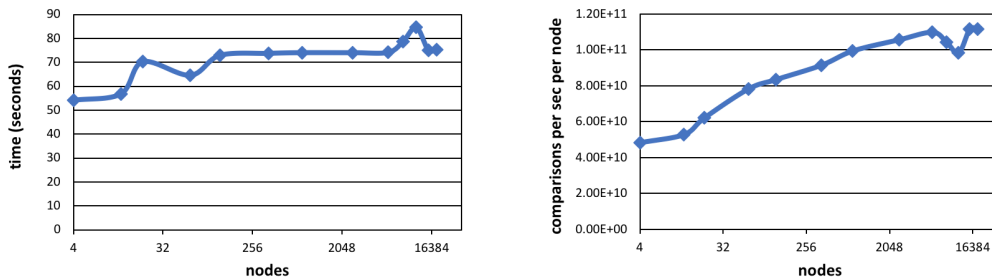


Figure 4: CCC 3-way weak scaling. Left: time to solution. Right: number of unique elementwise comparisons per second per node.

Table 3 shows the maximum operation and comparison rates attained at the highest node counts, up to 2.06 3-way petacomparisons per second.

### 6.6. Comparison with other work

We now compare against results reported in the literature as described in Section 1. We consider the most relevant comparable work we are aware of as of this writing. Table 4 shows comparisons per second for alternative methods and implementations. Unfortunately it is difficult to make rigorous comparisons when architectures and algorithms are significantly different and source code for the methods is not available or is not easily ported and tuned to a single common architecture for comparison. As a rough measure, a normalized performance ratio is calculated by normalizing the (absolute) comparison rate against the floating point rate of the respective hardware. For newer hardware, the double precision peak rate is used; for older GPUs with weak or nonexistent double precision support, single precision is used. This is used as a proxy for performance of bitwise integer operations required for the core metrics calculations on the respective processors, as this information typically is not readily available.

Table 4: Comparisons to related work

code	problem	node config	nodes used	GFlop rate	cmp/sec ( $\times 10^9$ )	norm perf
[12]	2-way 1-bit	1 Intel Core i7-920	1	42.56 DP	222	5.216
GBOOST[7]	2-way GWAS	1 NVIDIA GTX 285	1	1062.72 SP	64.08	.060
GWISFI[8]	2-way GWAS	1 NVIDIA GTX 470	1	1088.6 SP	767	.705
[15]	2-way GWAS	1 NVIDIA GTX 470	1	1088.6 SP	649	.596
[12]	2-way 1-bit	1 NVIDIA GTX 480	1	1345 SP	1185	.881
[15]	2-way GWAS	IBM Blue Gene/Q	4096	839e3 DP	2520	.003
epiSNP[16]	2-way GWAS	2 Intel Xeon Phi SE10P	126	271e3 DP	1593	.006
[9]	2-way GWAS	2 NVIDIA K20m + 1 Intel Xeon Phi 5110P	1	3360.56 DP	1053	.313
CoMet	2-way CCC	1 NVIDIA K20X	17955	26.0e6 DP	9.110e6	.350
GPU3SNP[10]	3-way GWAS	4 NVIDIA GTX Titan	1	6000 DP	264.7	.044
CoMet	3-way CCC	1 NVIDIA K20X	18424	26.7e6 DP	2.060e6	.077

We consider first the total number of comparisons per second. Table 4 demonstrates that the CoMet code used in the present work gives several orders of magnitude higher absolute performance, as measured in comparisons per second, far beyond the demonstrated capability of any other code.

The normalized performance ratio of CoMet is similar to or better than any result shown for other Kepler generation GPUs. Normalized performance of CoMet is also within the general range of demonstrated performance for cases using older Fermi GPUs, though it is not always the fastest case by this rough measure. It is unclear to what extent architectural differences between the GPUs account for this. Also, some other codes use a 3-bit representation of alleles rather than the 2-bit representation used here; this requires 50% more storage but may result in higher performance than the present implementation. Additionally, the CPU results of [12] are far faster than any other method, however this is because their algorithm only compares single bits rather than all combinations of 2 or 3 bits per element as is done for the other cases. A topic of future work will be to investigate further performance optimizations for the present code. In any case, it should be noted that since CoMet has similar relative performance to codes like [8], and since those codes already outperform conventional non-GPU methods by whole orders of magnitude (see [8] for details), the same is necessarily true of CoMet.

## 7. Future work

The CoMet code here described will be used in a 2018 Department of Energy (DOE) INCITE project on the ORNL Titan system, whose purpose is to study genetic characteristics of *Populus* species with applications to production of cellulosic biomass fuels [27]. The transition of CoMet to production use for this and other projects has necessitated ongoing development in the following areas.

1. Real-world genomic data is oftentimes sparse due to missing data at some allele locations. The approach described earlier can be modified for this case in a straightforward fashion. Since the input vector values (0, 1) and (1, 0) have an identical effect on the calculated result, the value (1, 0) can be set aside as a marker to denote a missing entry in the input vector. The same approach described earlier using (1, 0) as a marker for skipping a calculation for the 3-way case can readily be adapted to skipping calculations for missing entries in the sparse case. Preliminary test show performance of the associated modified GEMM kernel is only 9% less than the mGEMM3 rate shown in Table 2.
2. Our current model is designed for biallelic SNP data, in which each marker has two states, either two nucleotide states or insertion/deletion states, and we omit multi-allelic SNPs. 2-way CCC in our current modeling returns four values, representing the four possible combinations that a biallelic

variable can assume. In our future work, we plan to extend our CCC measure to allow an arbitrary number of marker states. When computing the correlation for a marker with  $s_1$  states and a marker with  $s_2$  states, CCC will compute the  $s_1 \times s_2$  possible relationships and return a matrix with  $s_1 \times s_2$  values, at higher computational expense than the current approach. The network model will have  $s_1$  and  $s_2$  nodes for the first and second markers, respectively.

3. To address instances of the 2-way case for which the results are too large to fit into system memory, a “phase” technique can be implemented, analogous to the staging technique described earlier for the 3-way case. Specifically, each processor’s blocks of computed metrics results are assigned phase numbers in a round-robin fashion for a specified number of phases, and a single run of the code will compute and store only a single phase of results at a time. The same approach can also reduce memory pressure for the 3-way case in addition to the staging option.
4. Past experience with other codes has shown that permuting the process axis order for codes with multidimensional parallelism may improve performance, by mapping processes with higher communication bandwidth requirements to processors physically closer in the system’s interconnect topology. In particular, for systems with multiple GPUs per node, mapping the field processor axis (which has high parallel reduction demands) to be in-node may be beneficial to performance.
5. The required genomics calculations are highly I/O intensive. Experiments have shown that preprocessing the input data into a single packed binary file and allowing each compute node to read its required portion from that file performs well in practice.
6. Potentially vast quantities of output may be produced. However in practice it is often the case that very few of the elements are actually needed—only those above a certain threshold size, which may amount to less than one millionth of the calculated values. Tests have shown that in this regime it is efficient for each compute node to write its results to a separate small file. To load balance the output, it is advantageous to randomly permute the vectors of the input file as an offline preprocessing step. This removes correlations between the parallel decomposition and the distribution of similar vectors in the input data. One small file per process should also be effective for burst buffer hardware being delivered in newer HPC systems.
7. It is likely that further code optimizations are possible, for example, improving the performance of the mGEMM2/mGEMM3 operations and reducing other overheads.
8. Porting to other architectures including pre-exascale and exascale platforms is expected to be tractable. Support of Intel Xeon Phi nodes by modification of open source dense linear algebra libraries is a possible option.

Table 5. shows preliminary results with CoMet on the ORNL Summit system [28]. In its final form Summit will be a 200 petaflop system with 4,608 compute nodes, each node composed of two IBM Power9 processors and six NVIDIA Volta GPUs. The experiments in Table 5 apply the 2-way CCC method to a synthetic dataset with 141,714 vectors of length 882 or 358,000 entries. Comparisons with Titan are also shown, using 30 GPUs in both cases, also with comparison to the corresponding CPU-only case. The Summit vs. Titan per-GPU performance ratio for a large problem that saturates both systems’ GPUs is 6.44X, slightly exceeding the roughly 5X peak flop rate ratio of the two GPU models, most likely due to architectural improvements in the Volta GPU. The smaller vector length 882 case does not saturate the GPU as well; here the per-GPU performance of Summit exceeds Titan by a smaller factor. The Summit GPU / CPU performance ratio is 119.2X, exceeding the roughly 40X peak flop rate ratio between the six GPUs and the two CPUs of each node, this being expected since the CPU code version is not as heavily optimized as the GPU version. The largest Summit case shown here attains 3.328e12 comparisons per second per GPU. This rate extrapolated linearly to the eventual full Summit system yields an estimate of 92.0 petacomparisons per second, an unprecedented scale.

## 8. Conclusions

We have defined a new set of algorithm implementations for performing 2-way and 3-way Custom Correlation Coefficient calculations for comparative genomics applications. Performance of up to nine quadrillion

Table 5: Summit vs. Titan performance, 30 GPUs, 30 Titan nodes, 5 Summit nodes; runtimes in seconds

system	Titan	Summit	ratio	Titan	Summit	ratio
vector length	882	882		358,000	358,000	
GPU	5.63	1.86	3.02X	232	36.0	6.44X
CPU	—	222.3	—	—	—	—
ratio	—	119.2X	—	—	—	—

vector element comparisons per second is demonstrated. To our knowledge this is the first simulation of its kind ever performed at this scale, demonstrating the capability to perform simulations that were until recently considered far beyond what is possible, enabling new kinds of science in comparative genomics.

## Acknowledgments

This research used resources of the Oak Ridge Leadership Computing Facility at the Oak Ridge National Laboratory, which is supported by the Office of Science of the U.S. Department of Energy under Contract No. DE-AC05-00OR22725.

Funding provided by The BioEnergy Science Center (BESC) and The Center for Bioenergy Innovation (CBI). U.S. Department of Energy Bioenergy Research Centers supported by the Office of Biological and Environmental Research in the DOE Office of Science.

Support for the Poplar GWAS dataset was provided by The BioEnergy Science (BESC) and The Center for Bioenergy Innovation (CBI). U.S. Department of Energy Bioenergy Research Centers supported by the Office of Biological and Environmental Research in the DOE Office of Science. The Poplar GWAS Project used resources of the Oak Ridge Leadership Computing Facility and the Compute and Data Environment for Science at Oak Ridge National Laboratory, which is supported by the Office of Science of the U.S. Department of Energy under Contract No. DE-AC05-00OR22725.

This research was also supported by the Plant-Microbe Interfaces Scientific Focus Area (<http://pmi.ornl.gov>) in the Genomic Science Program, the Office of Biological and Environmental Research (BER) in the U.S. Department of Energy Office of Science. Oak Ridge National Laboratory is managed by UT-Battelle, LLC, for the US DOE under contract DE-AC05-00OR22725.

This research was also supported by the Department of Energy Laboratory Directed Research and Development funding (7758), at the Oak Ridge National Laboratory. Oak Ridge National Laboratory is managed by UT-Battelle, LLC, for the US DOE under contract DE-AC05-00OR22725.

We would like to acknowledge Gerald Tuskan, Stephen DiFazio and the DOE Joint Genome Institute (JGI) for sequencing the *Populus* genotypes and generating the processed SNP data.

## References

- [1] S. Climer, W. Yang, L. de las Fuentes, V. G. Davila Roman, C. C. Gu, A Custom Correlation Coefficient (CCC) Approach for Fast Identification of Multi-SNP Association Patterns in Genome-Wide SNPs Data, *Genetic Epidemiology* 38 (7), <http://www.ncbi.nlm.nih.gov/pubmed/25168954>. [Online; accessed 1-March-2016].
- [2] S. Climer, A. R. Templeton, W. Zhang, Allele-specific network reveals combinatorial interaction that transcends small effects in psoriasis gwas, *PLoS Comput Biol* 10 (9) (2014) e1003766.
- [3] D. Tiosano, L. Audi, S. Climer, W. Zhang, A. R. Templeton, M. Fernández-Cancio, R. Gershoni-Baruch, J. M. Sánchez-Muro, M. El Kholy, Z. Hochberg, Latitudinal clines of the human vitamin D receptor and skin color genes, *G3: Genes—Genomes—Genetics* 6 (5) (2016) 1251–1266.
- [4] K. A. Frazer, D. G. Ballinger, D. R. Cox, D. A. Hinds, L. L. Stuve, R. A. Gibbs, J. W. Belmont, A. Boudreau, P. Hardenbol, S. M. Leal, et al., A second generation human haplotype map of over 3.1 million SNPs, *Nature* 449 (7164) (2007) 851–861.
- [5] S. Climer, A. R. Templeton, W. Zhang, Human gephyrin is encompassed within giant functional noncoding yin-yang sequences, *Nature communications* 6.
- [6] W.-H. Wei, G. Hemani, C. S. Haley, Detecting epistasis in human complex traits, *Nature Reviews Genetics*, <http://www.nature.com/nrg/journal/v15/n11/full/nrg3747.html>. [Online; accessed 11-October-2016].

- [7] L. S. Yung, C. Yang, X. Wan, W. Yu, GBOOST: a GPU - based tool for detecting gene gene interactions in genome wide case control studies, *Bioinformatics* 27 (9) (2011) 1309–1310.  
URL <http://bioinformatics.oxfordjournals.org/content/27/9/1309.abstract>
- [8] Q. Wang, F. Shi, A. Kowalczyk, R. M. Campbell, B. Goudey, D. Rawlinson, A. Harwood, H. Ferra, A. Kowalczyk, GWISFI: A universal GPU interface for exhaustive search of pairwise interactions in case-control GWAS in minutes, in: 2014 IEEE International Conference on Bioinformatics and Biomedicine, 2014, , <http://ieeexplore.ieee.org/document/6999192>. [Online; accessed 11-October-2016].
- [9] J. Gonzalez-Dominguez, S. Ramos, J. Tourino, B. Schmidt, Parallel Pairwise Epistasis Detection on Heterogeneous Computing Architectures, *IEEE Transactions on Parallel and Distributed Systems*, <http://ieeexplore.ieee.org/document/7165657/>. [Online; accessed 11-October-2016].
- [10] J. Gonzalez-Dominguez, B. Schmidt, GPU-accelerated exhaustive search for third-order epistatic interactions in casecontrol studies, *Journal of Computational Science* 8 (2015) 93 – 100. doi:<http://dx.doi.org/10.1016/j.jocs.2015.04.001>.  
URL <http://www.sciencedirect.com/science/article/pii/S1877750315000393>
- [11] E. Solomonik, D. Matthews, J. Hammond, J. Demmel, Cyclops Tensor Framework: Reducing communication and eliminating load imbalance in massively parallel contractions, in: Parallel Distributed Processing (IPDPS), 2013 IEEE 27th International Symposium on, 2013, pp. 813–824, , <http://ieeexplore.ieee.org/document/6569864/?arnumber=6569864>. [Online; accessed 11-October-2016]. doi:10.1109/IPDPS.2013.112.
- [12] I. S. Haque, V. S. Pande, W. P. Walters, Anatomy of High-Performance 2D Similarity Calculations, *Journal of Chemical Information and Modeling* 51 (9) (2011) 2345–2351.  
URL <http://dx.doi.org/10.1021/ci200235e>
- [13] Z. Wang, Y. Wang, K.-L. Tan, L. Wong, D. Agrawal, eCEO: an efficient Cloud Epistasis cOmputing model in genome-wide association study, *Bioinformatics* 27 (8) (2011) 1045–1051. arXiv:<http://bioinformatics.oxfordjournals.org/content/27/8/1045.full.pdf+html>, doi:10.1093/bioinformatics/btr091.  
URL <http://bioinformatics.oxfordjournals.org/content/27/8/1045.abstract>
- [14] J. C. Yang, C. Harris, S. Young, G. Morahan, Adapting Genome-Wide Association Workflows for HPC Processing at Pawsey, in: Supercomputing SC15, 2015, , [http://sc15.supercomputing.org/sites/all/themes/SC15images/tech\\_poster/tech\\_poster\\_pages/post200.html](http://sc15.supercomputing.org/sites/all/themes/SC15images/tech_poster/tech_poster_pages/post200.html). [Online; accessed 11-October-2016].
- [15] B. Goudey, M. Abedini, J. L. Hopper, M. Inouye, E. Makalic, D. F. Schmidt, J. Wagner, Z. Zhou, J. Zobel, M. Reumann, High performance computing enabling exhaustive analysis of higher order single nucleotide polymorphism interaction in Genome Wide Association Studies, in: Proceedings of the HISA BIG DATA 2013 Conference, 2015, , <https://link.springer.com/article/10.1186/2047-2501-3-S1-S3>. [Online; accessed 5-February-2018].
- [16] G. R. Luecke, N. T. Weeks, B. M. Groth, M. Kraeva, L. Ma, L. M. Kramer, J. E. Koltjes, J. M. Reecy, Fast Epistasis Detection in Large-Scale GWAS for Intel Xeon Phi Clusters, in: Trustcom/BigDataSE/ISPA, 2015 IEEE, 2011, , <http://ieeexplore.ieee.org/document/7345653/>. [Online; accessed 11-October-2016].
- [17] N. T. Weeks, G. R. Luecke, B. M. Groth, M. Kraeva, L. Ma, L. M. Kramer, J. E. Koltjes, J. M. Reecy, High-performance epistasis detection in quantitative trait GWAS, *The International Journal of High Performance Computing Applications* 0 (0) (0) 1094342016658110.  
URL <http://dx.doi.org/10.1177/1094342016658110>
- [18] L. Koesterke, D. Stanzione, M. Vaughn, S. M. Welch, W. Kusnierczyk, An Efficient and Scalable Implementation of SNP-Pair Interaction Testing for Genetic Association Studies, in: 2011 IEEE International Parallel and Distributed Processing Symposium, 2011, , <http://ieeexplore.ieee.org/document/6008872/>. [Online; accessed 11-October-2016].
- [19] J. Johnson, M. Douze, H. Jegou, Billion-scale similarity search with GPUs, <https://arxiv.org/abs/1702.08734>. [Online; accessed 10-May-2017].
- [20] W. Joubert, J. Nance, D. Weighill, D. Jacobson, Parallel Accelerated Vector Similarity Calculations for Genomics Applications, *Parallel Computing* 75, <https://www.sciencedirect.com/science/article/pii/S016781911830084X>.
- [21] S. Tomov, R. Nath, H. Ltaief, J. Dongarra, Dense linear algebra solvers for multicore with GPU accelerators, in: Parallel Distributed Processing, Workshops and Phd Forum (IPDPSW), 2010 IEEE International Symposium on, 2010, pp. 1–8, , [http://ieeexplore.ieee.org/xpls/abs\\_all.jsp?arnumber=5470941](http://ieeexplore.ieee.org/xpls/abs_all.jsp?arnumber=5470941). [Online; accessed 1-March-2016]. doi:10.1109/IPDPSW.2010.5470941.
- [22] M. Beeler, R. W. Gosper, R. Schroepel, HAKMEM, 1972.
- [23] H. S. Warren, *Hacker’s Delight* (2nd ed.), Addison Wesley, 2012.
- [24] PLASMA, <http://icl.cs.utk.edu/plasma/software>. [Online; accessed 11-October-2016].
- [25] BLIS, <https://github.com/flame/blis>. [Online; accessed 11-October-2016].
- [26] OpenBLAS: An optimized BLAS library, <http://www.openblas.net/>. [Online; accessed 11-October-2016].
- [27] DOE INCITE 2018 Fact Sheet, <http://www.doeleadershipcomputing.org/awards/2018INCITEFactSheets.pdf>. [Online; accessed 3-February-2018].
- [28] Summit, <https://www.olcf.ornl.gov/summit>. [Online; accessed 3-February-2018].